Asian Journal of Chemistry; Vol. 33, No. 3 (2021), 671-676

ASIAN JOURNAL OF CHEMISTRY

https://doi.org/10.14233/ajchem.2021.23032

Synthesis and Characterization of Chitosan-Polyaniline-Manganese Dioxide Nanocomposite for Removal of Methyl Orange Dye

B.R.S. RATHORE[1], N.P.S. CHAUHAN[2], M.K. RAWAL[3], S.C. AMETA[1] and R. AMETA[1,4,*]

[1]Department of Chemistry, PAHER University, Udaipur-313003, India
[2]Department of Chemistry, Faculty of Science, Bhupal Nobles's University, Udaipur-313002, India
[3]Department of Chemistry, Vidya Bhawan Rural Institute, Udaipur-313002, India
[4]Department of Chemistry, J.R.N. Rajasthan Vidyapeeth (Deemed to be University), Udaipur-313001, India

*Corresponding author: E-mail: rakshit_ameta@yahoo.in

Received: 18 October 2020; *Accepted*: 30 January 2021; *Published online*: 16 February 2021; AJC-20267

An ecofriendly polymer composite based on chitosan, polyaniline and manganese dioxide has been prepared using batch adsorption method and analyzed by Fourier transform infrared (FTIR), UV-vis, X-ray diffraction (XRD), scanning electron microscopy (SEM) and transmission electron microscopy (TEM). FTIR results suggested the presence of functional groups like hydroxyl and amino groups and also shown a significant shift in IR bands in CS-PANI-MnO_2 composite. The surface of composite was quite rough within the folds of pleated regions as observed from the SEM and TEM morphologies. The prepared composite was also utilized as an adsorbent for the treatment of methyl orange from the aqueous solution and achieved a reasonably good adsorption capacity of 96.2%. The biochemical oxygen demand (BOD) and chemical oxygen demand (COD) tests also suggested their suitability for the adsorption of methyl orange dye.

Keywords: Polyaniline, Chitosan, MnO_2, Nanocomposites, Adsorption, Dye degradation.

INTRODUCTION

Industrial wastewater with organic pollutants has become one of the most serious problems related to environment. One conceivable treatment is to develop an effective and environmental friendly material to degrade the organic pollutant. Polymer metal oxide composite with a structural regularity and synthetic stability may provide an important alternate to perform degradation [1]. To combat this issue, advanced oxidation processes (AOPs), where semiconductor photocatalysts are utilized, is viewed as the best one among present different strategies. Nath *et al.* [2] have developed green, sustainable environmentally benign and industrially viable polymeric heterogeneous catalysts for degradation of versatile wastewater organic contaminants. Sani *et al.* [3] have synthesized polymer coated ZnO with chitosan nanocatalyst using microwave hydrothermal method for the removal of methylene blue dye from synthetic wastewater, which showed a good adsorption ability as compared to ordinary ZnO.

Mozafari & Chauhan [4] reported various synthetic routes of polyaniline, functionalized polyaniline and its nanocomposites with chitosan and metal oxides. As the need to use green chemistry routes is increasing, new environmentally friendly catalytic processes are in demand. Chatterjee *et al.* [5] synthesized PANI-SWCNT composites for the degradation of rose Bengal and methyl orange dyes. Moreover, other dyes, *viz.* Congo red, coomassie brilliant blue, remazol, brilliant blue R and methylene blue from aqueous solution can be removed using polyaniline/chitosan composite [6]. Gemeay *et al.* [7] studied the degradation of acid blue 25 dye (AB-25) using polyaniline/manganese dioxide (PANI/MnO_2), whereas Zhong *et al.* [8] developed an composite electrode where polyaniline (PANI) was embeded into petaline NIO (niO@PANI-CF) and observed that reactive brilliant red X-3B dye degration and COD extraction effectiveness exceeded to 95.94 and 64.24% at 48 h, respectively. Sultana *et al.* [9] prepared polyaniline grafted chitosan copolymer *via in situ* polymerization of anilines using ammonium persulfate as initiators while silver nanoparticles were integrated into a polymer matrix by a chemical reduction method.

Due to its high adsorption capacity and macromolecular structure, chitosan when combined with high conductivity

material PANI has proved to be a potential composite for the removal of the dyes in aqueous solution efficiently. Mohammadi *et al*. [10] developed a chitosan-polyaniline composite with a reasonable antibacterial, mechanical and electrical property in food packing materials, while some researchers also synthesized polyaniline-chitosan composite films for biomedical applications [11,12]. In extension of the better hybrid nanocomposite, the performance of chitosan and polyaniline depends on the structural modification and surface chemistry by incorporating nano-metal oxides. Vellakkat & Hundekkal [13] synthesized a chitosan, polyaniline and Co_3O_4 based nanocomposite using *in situ* chemical oxidation method for supercapacitor electrode applications and degradation of methylene blue dye. Similarly, polyaniline ZnO/chitosan nanocomposite was applied for the degradation of reactive orange-blue or methylene blue dye having a removal efficiency of 96 and 88.5%, respectively [14]. Keeping in view of above these facts, in present work, a novel nanocomposite based on chitosan, conducting PANI and MnO_2 has been synthesized and characterized by various tools such as XRD, FT-IR, UV-VIS, SEM, TEM, *etc.* for removal of methyl orange dye.

EXPERIMENTAL

Analytical grade chemicals were used throughout the experiments. Chitosan (100%), ammonium persulfate (APS) and methyl orange were purchased from Himedia, India while aniline, manganese nitrate and oxalyl dihydrazide were procured from Merck, India. For the preparation of all the solutions, double-distilled water was used.

Preparation of MnO_2 nanopowder: Manganese nitrate (as an oxidizing reagent) and oxalyl dihydrazide (as a reducing agent) were mixed with minimum quantities in deionized water with continuous stirring and then introduced into muffle furnace at 400 ºC. In this redox mixture, initially, dehydration takes place and then large amount of gases are evolved, which results in the production of froth, forming black porous foam. This foam was finally ground to obtain fine powder form of MnO_2.

Preparation of chitosan-polyaniline (CS-PANI) composites and chitosan-polyaniline-MnO_2 (CS-PANI-MnO_2) nanocomposites: CS-PANI was synthesized by using batch adsorption method as per reported [15] method. For CS-PANI-MnO_2, 5.0 g $MnCl_2$ along with 1.0 g MnO_2 was taken in 0.1 L water and then added into polyaniline-chitosan composite, dropwise along with the ammonium persulphate as an oxidant. This mixture was heated to 70 ºC for 2 h and then cooled for 3 h in an ice bath.

Characterization: FT-IR spectrometer (Perkin Elmer, USA) and UV VIS-NIR spectrohotometer Lambda 750 (Perkin Elmer, USA), XRD pattern measurement (Table Top X-ray Diffraction System, Rigaku Miniflex, USA), scanning electron microscopy (SEM) using a JEOL JSM-6100 microscope (Tokyo, Japan) and Transmission electron microscope-Tecnai 20 (Philips, Holland) were employed for study of structures and topographical studies of the nanocomposite.

Adsorption experiments, photocatalytic degradation and regeneration and recyclability studies of the synthesized CS-PANI-MnO_2 nanocomposite were preformed according to the known procedure [15].

RESULTS AND DISCUSSION

FTIR spectra: The FTIR spectra of chitosan, PANI, MnO_2, CS-PANI and CS-PANI-MnO_2 nanocomposite are shown in Fig. 1. A band appeared at 3454 cm^{-1} due to the combined peak of -OH and N-H stretching vibrations. A peak at 2923 cm^{-1} was attributed due to the symmetric -CH_2- stretching vibration of the pyranose ring [16]. A peak at 1156 cm^{-1} was attributed to the structure of chitosan, while the sharp peak at 1384 cm^{-1} was assigned to -CH_3 in alkyl substituted amide group [17-19]. The broad peaks at 1021 and 1098 cm^{-1} showed the C-O stretching vibration in chitosan whereas the peaks at 1614.6 and 1531 cm^{-1} were attributed to -C=O and N-H stretching, respectively. The absorption bands at 1138 cm^{-1} was attributed to the counter symmetric stretching of C-O-C links and 1096 and 1025.4 cm^{-1} were assigned to the skeletal vibrations including the C-O stretching. A characteristic band at 1583 cm^{-1} showed nitrogen bond among benzenoid and quinoid rings [4,20]. The band at 1668 cm^{-1} is related to C=C extending (phenyl ring). The peak at 1305 cm^{-1} is attributed to C-N stretching of tertiary aromatic amine, similarly a band at 815 cm^{-1} is expected to an aromatic =C-H plane twisting. This shows great agreements with the results reported by Chauhan *et al.* [21]. The broad band at 3256 cm^{-1} is attributed to the stretching vibrations of hydrogen bonded surface water molecule and hydroxyl groups of the compound. Additionally, the bands at 1645 and 1386 cm^{-1} correspond to the existence of large numbers of residual hydroxyl groups, which imply the O-H vibrating mode of traces of adsorbed water [22].

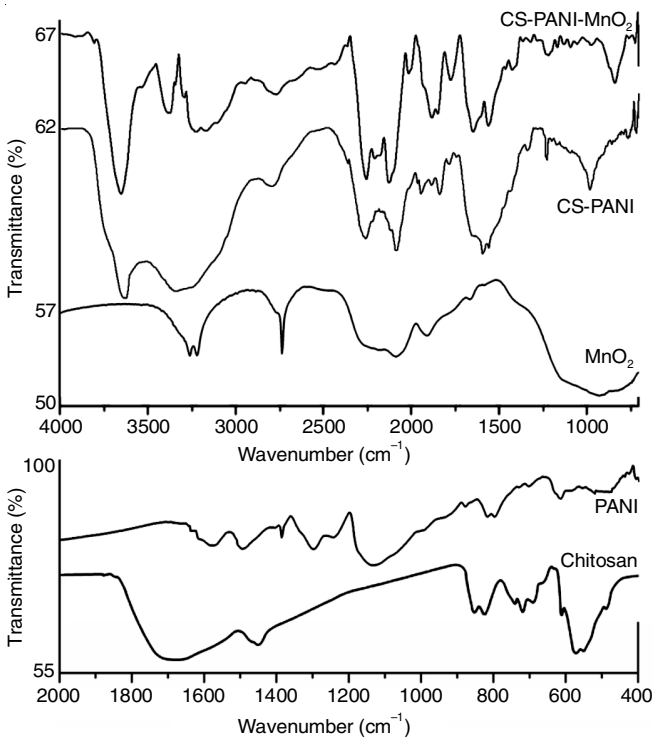

Fig. 1. FT-IR spectra of chitosan, PANI, MnO_2, CS-PANI and CS-PANI-MnO_2

The band at 560 cm^{-1} can be attributed to the Mn-O vibrations of MnO_2 nanopowder [23,24]. For CS-PANI-MnO_2, chitosan, PANI and MnO_2, IR range has been shifted, however every group has somewhat changed and the quinoid band intensity and the C-H twist mode have changed. The peaks for CS-PANI-MnO_2 composites were found at 3440, 2990.8, 1623, 1521, 1331, 1145 and 617 cm^{-1}.

UV spectra: Chitosan gives an absorption spectrum which is a characteristic for chitosan and shows no peaks at 350-800 nm. Pure PANI reported two bands in the spectrum of absorption from 425 to 475 is attributed to π-π* transition of benzenoid and 500 to 750 nm due to π-π* transition of quinoid [25]. PANI showed three peaks, first at ~210 nm due to π-π* transition, second at 430 nm and a broader peak in the range 595 to 750 nm. The electronic transition appears at 455 nm is attributed to n-π* for nanocomposite. The shift to a higher wavelength region suggests that the interaction between metal oxide and PANI occurs through quinoid (require less energy than benzenoid) [26] (Fig. 2). A broad peak in the range 600 to 750 nm might be due to the exciton like transition in quinoid units [27,28].

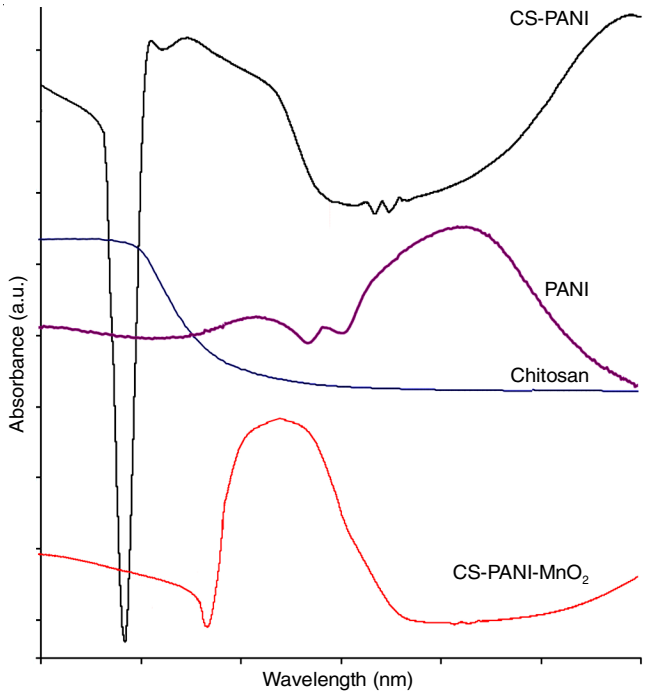

Fig. 2. UV-vis spectra of chitosan, PANI, CS-PANI and CS-PANI-MnO_2

XRD analysis: The 2θ values in between 10º and 20º in XRD pattern for chitosan, which is probably attributed to the hydrogen bonding in between –OH and –NH_2 groups. The peaks at 2θ = 9.79º, 14.38º, 19.5º and 24.9º are the characteristic of PANI [27]. The peaks at 9.9º, 19.2º and 25.3º are the characteristic assignments of the PANI (Fig. 3).

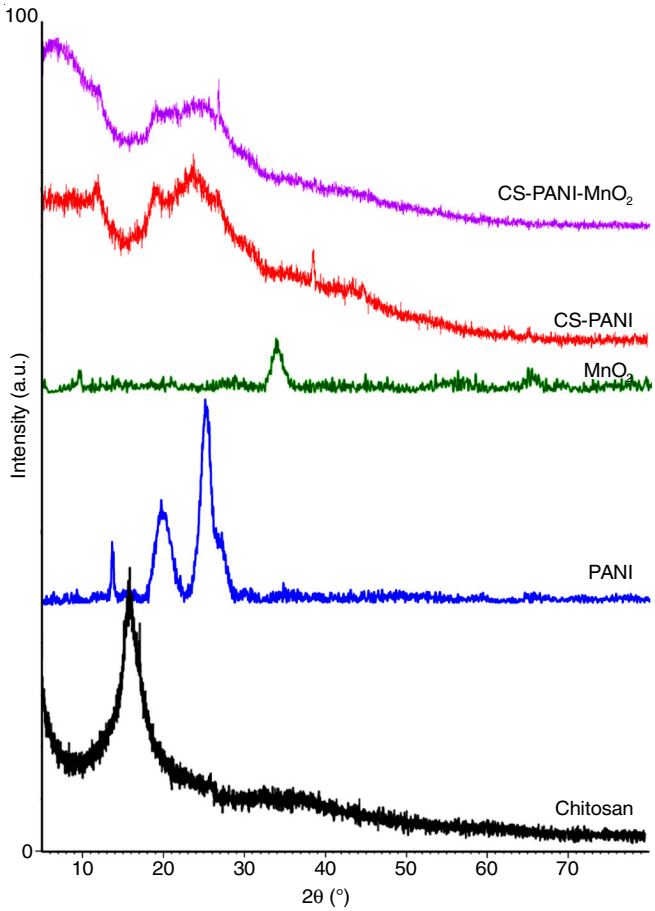

Fig. 3. XRD of chitosan, PANI, MnO_2, CS-PANI and CS-PANI-MnO_2

The peaks observed at 24º, 27º, 35º, 39º, 43º and 52º are the characteristics peak of pure MnO_2 nanoparticles. The peaks corresponded to the (2 2 0), (3 1 0), (4 0 0), (3 3 0), (3 0 1) and (4 1 1) of a tetragonal structure of pure MnO_2 nanoparticles. In present study, the Scherrer's equation was used to calculate the average particle size [29,30]. The average crystalline size of MnO_2 nanoparticle was found as 20 nm. The diffraction data for both compounds are tabulated in Table-1, which are in good

TABLE-1
XRD DATA CS-PANI COMPOSITE AND CS-PANI-MnO_2 NANOCOMPOSITES

CS-PANI composite				CS-PANI-MnO_2 nanocomposite			
Position [2θ]	FWHM [2θ]	d-spacing [Å]	Relative intensity [%]	Position [2θ]	FWHM [2θ]	d-spacing [Å]	Relative intensity [%]
11.7336	0.6691	7.54220	91.88	5.3389	0.6691	16.55303	7.87
23.5509	0.4015	3.77769	66.64	12.0897	0.4015	7.32087	45.48
26.7556	0.6691	3.33204	38.40	18.8480	0.8029	4.70833	38.66
38.4996	0.2342	2.33839	100.00	26.7188	0.1338	3.33655	100.00
44.6730	0.4015	2.02854	39.93	38.6897	0.2342	2.32733	16.03
62.9418	0.8029	1.47670	15.26	–	–	–	–
65.1552	0.4015	1.43179	23.78	–	–	–	–

agreement with the other diffractions peaks of chitosan, polyaniline and MnO_2. Thus, the successful formations of nanocomposites of MnO_2 and CS-PANI have been established by XRD analysis.

Morphological studies: Figs. 4 and 5 show the SEM and TEM images of the CS-PANI composites and CS-PANI-MnO_2 nanocomposites, which confirm their diameters as 75.5 and 13.5 nm, respectively (Fig. 4a & c). Moreover, it has been found that spherical agglomerated consistently packed particles of diameter under 200 nm are shown at few regions. A uniform morphology and substance homogeneity observed in this case provides an edge over other synthetic routes for interfacial polymerization.

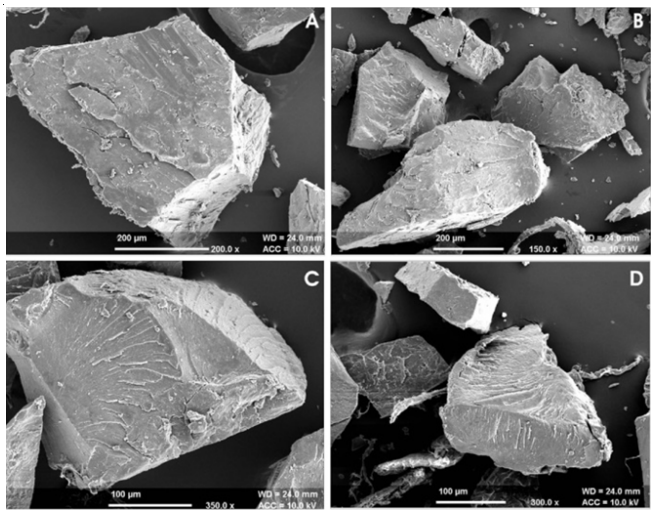

Fig. 4. SEM of CS-PANI composite (a) and (b) and CS-PANI-MnO_2 nanocomposite (c) and (d)

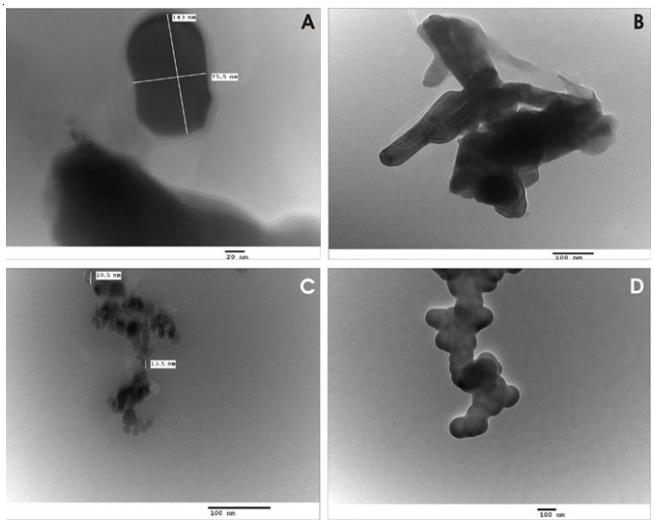

Fig. 5. TEM of CS-PANI composite (a) and (b) and CS-PANI-MnO_2 nanocomposite (c) and (d)

Adsorption studies: The adsorption studies of methyl orange dye on CS-PANI composite and CS-PANI-MnO_2 nanocomposite at different initial concentration, pH and dosage of adsorption were analyzed as a function of contact time to depict the equilibrium time.

Maximum removal of the dye on to the nanocomposite and composite at pH 3 was found to be 98 and 68.8%, respectively (Fig. 6a). It may be attributed to the protonation of functional group such as amino and hydroxyl group, which increases the electrostatic interaction between the positively charge adsorbent surface and negatively charge dye molecule. However, at the low adsorption from pH 6 to 9 was due to the presence of excess of OH^- ions and deprotonation of the functional group, which reduces the electrostatic interaction between the adsorbent and adsorbate. A negative charged surface on the adsorbent dose doesn't favour the adsorption of anionic dye molecule. Due to the electrostatic repulsion with pH more than 9, the adsorption of dye increases again as depicted in Fig. 6a. So, it is concluded from these results, that with the introduction of MnO_2 on to the CS-PANI composite availability of active site is more for methyl orange dye because of the larger surface area as compared with CS-PANI composite. Hence, this form of hybrid material's low cost and high extraction rate made it a successful candidate to extract the dye from the effluent.

Fig. 6b shows the time course of the adsorption equilibrium for CS-PANI-MnO_2 nanocomposite and Fig. 6c gives an idea about the adsorption equilibrium of methyl orange on to CS-PANI composite. The extraction of methyl orange was very fast in the first 5 min and then declines gradually with time changes up to equilibrium. The improvement in adsorption behaviour in the initial state can be due to additional adsorption site present on the surface of nanocomposite CS-PANI-MnO_2. Then the rate of adsorption decreases the amount of methyl orange colour adsorbed onto the composite and the amount of colour adsorbed from the composite is in dynamic equilibrium. The time required to achieve this state of equilibrium was referred to as the equilibrium time and the amount of dye adsorbed at the equilibrium time represented the optimum adsorption capacity of the adsorbent under experimental conditions. The contact time expected for the CS-PANI-MnO_2 nanocomposite was about 45 min for methyl orange equilibrium condition and about 50 min for CS-PANI composite. The time required to attend the equilibrium is almost the same as that reported by Kannusamy & Sivalingam [31].

At lower concentration, dye solution 20 mg L^{-1} have the removal efficiency about 94.1 and 81.6% for CS-PANI-MnO_2 nanocomposite and CS-PANI composite, respectively (Fig. 6c-d). The enhanced removal of methyl orange colour at the low concentration could be attributed to a more rapid move-ment of the dye in both sites; nanocomposite and composite at higher concentration of dye (500 mg L^{-1}). The removal rate was decreased to 29.3 for CS-PANI-MnO_2 nanocomposite and 20.5% for CS-PANI composite (Fig. 6d-e).

Photocatalytic activity: A comparison of CS-PANI-MnO_2 nanocomposite and CS-PANI composite according to their photocatalytic activity are shown in Fig. 7. Few sets of experiment were performed. In first set, dye degradation in UV light and without catalyst and the decolourization efficiency was 2.5% after 1.5 h irradiation. The second set was performed in dark condition in the presence of catalyst with dye sample for both; nanocomposite and composite, the decolourization

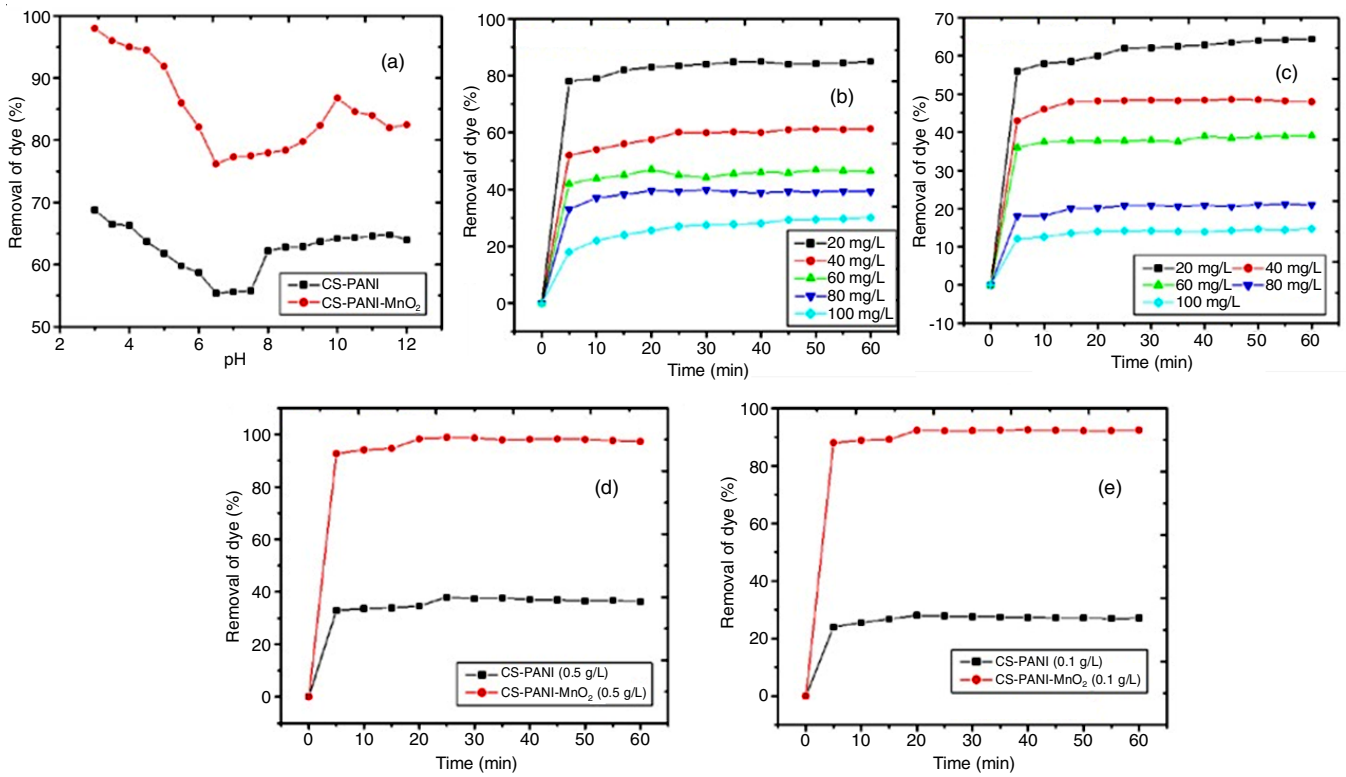

Fig. 6. Effect of contact time on dye removal efficiency for CS-PANI and CS-PANI-MnO_2 nanocomposite: (a) pH for CS-PANI and CS-PANI-MnO_2 (b) CS-PANI-MnO_2 for different dosage concentration (c) CS-PANI for different dosage concentration (d) CS-PANI and CS-PANI-MnO_2 at concentration of 0.5 g L^{-1} and (e) CS-PANI and CS-PANI-MnO_2 at concentration of 0.1 g L^{-1} [values are the mean of n = 3 (mean ± standard error)]

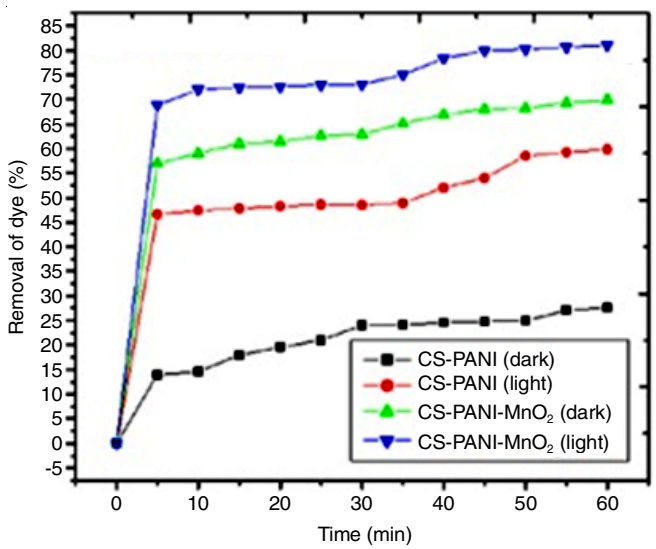

Fig. 7. Photocatalytic activity for CS-PANI and CS-PANI-MnO_2 in dark and light

efficiency 69.9 and 27.6%, respectively. Such results in dark are attributed to adsorption mechanism of catalyst. The third set of experiment was performed in the presence of UV light irradiation to observe interaction between dye and catalyst. The results clearly showed that CS-PANI-MnO_2 nanocomposite can enhance the catalytic activity in presence of CS-PANI composite for the degradation of the dye. Here, removal efficiency was found to be 81 and 59.8%, respectively.

COD and BOD removal: COD was estimated using potassium dichromate method. A sample solution was refluxed with known amount of $K_2Cr_2O_7$ in H_2SO_4 medium and excess of $K_2Cr_2O_7$ was treated against ferrous ammonium sulphate. The amount of $K_2Cr_2O_7$ consumed is directly proportional to the oxygen required to oxidize the oxidizable organic matter.

Increased contact time has resulted in an increase in the efficiency of COD removal. Initial COD value was found to be 340 mg L^{-1}, which was reduced to 272 mg L^{-1} for CS-PANI composite and 160 mg L^{-1} for CS-PANI-MnO_2 nanocomposite. The removal % of an initial dye concentration of 100 mg L^{-1} was found 50% for CS-PANI composite and 18% for CS-PANI-MnO_2 nanocomposite after 30 min. The removal % increases with the increasing contact time (up to 30 min), which clearly indicated that the nanocomposite has higher efficiency to degrade dye molecule into small organic molecules.

Similarly, BOD experiments were performed at 27 ºC for a three day of contact between the dye and synthesized nanocomposite (CS-PANI-MnO_2 nanocomposite and CS-PANI composite). The BOD for CS-PANI composite was found about 86 mg L^{-1}, while using CS-PANI-MnO_2 nanocomposite, BOD reduces to 56 mg L^{-1}. A reduction of BOD value also signifies the importance of the catalytic degradation treatment in light.

Conclusion

The CS-PANI composite and CS-PANI-MnO_2 nanocomposites were prepared and characterized using various techniques. The adsorption studies of methyl orange dye on CS-PANI and

CS-PANI-MnO_2 nanocomposite composites were performed and found that CS-PANI-MnO_2 nanocomposite was more efficient as compared to CS-PANI composite regarding removal of the dye. The removal efficiency for CS-PANI-MnO_2 and CS-PANI was found as 94.1 and 81.6%, respectively. The CS-PANI-MnO_2 nanocomposite has reasonably good catalyst compared to CS-PANI composite by photocatalytic degradation of methyl blue dye. The results of BOD and COD also suggest its suitability for removal of methyl orange dye.

ACKNOWLEDGEMENTS

The authors thank Sophisticated Analytical Instrumentation Facility (SAIF), Panjab University, Chandigarh, India, for providing the instrumentation facilities (SEM, TEM, FTIR and XRD).

CONFLICT OF INTEREST

The authors declare that there is no conflict of interests regarding the publication of this article.

REFERENCES

1. N. Jalali, G. Trujillo-de Santiago, M. Motevalian, M.Y. Karimi, N.P.S. Chauhan, Y. Habibi and M. Mozafari, *Biomimet. Nanobiomater.*, **5**, 74 (2016); https://doi.org/10.1680/jbibn.15.00016
2. I. Nath, J. Chakraborty, P.M. Heynderickx and F. Verpoort, *J. Appl. Catal. B*, **227**, 102 (2018); https://doi.org/10.1016/j.apcatb.2018.01.032
3. H. Sani, H. Aliyu and S. Tukur, *ISOR J. Appl. Chem.*, **8**, 34 (2015);
4. M. Mozafari and N.P.S. Chauhan, Advanced Functional Polymers for Biomedical Applications, Elsevier (2019).
5. M.J. Chatterjee, A. Ghosh, A. Mondal and D. Banerjee, *RSC Adv.*, **7**, 36403 (2017); https://doi.org/10.1039/C7RA03855K
6. V. Janaki, B.-T. Oh, K. Shanthi, K.-J. Lee, A.K. Ramasamy and S. Kamala-Kannan, *Synth. Met.*, **162**, 974 (2012); https://doi.org/10.1016/j.synthmet.2012.04.015
7. A.H. Gemeay, R.G. El-Sharkawy, I.A. Mansour and A.B. Zaki, *Bull. Mater. Sci.*, **35**, 585 (2012); https://doi.org/10.1007/s12034-012-0328-0
8. D. Zhong, X. Liao, Y. Liu, N. Zhong and Y. Xu, *Bioresour. Technol.*, **258**, 125 (2018); https://doi.org/10.1016/j.biortech.2018.01.117
9. S. Sultana, N. Ahmad, S.M. Faisal, M. Owais and S. Sabir, *IET Nanobiotechnol.*, **11**, 835 (2017); https://doi.org/10.1049/iet-nbt.2016.0215
10. B. Mohammadi, S. Pirsa and M. Alizadeh, *Polym. Polymer Compos.*, **27**, 507 (2019); https://doi.org/10.1177/0967391119851439
11. B. Pasela, A. Castillo, R. Simon, M. Pulido, H. Mana-ay, M. Abiquibil, R. Montecillo, K. Thumanu, D. von Tumacder and K. Taaca, *Biomimetics*, **4**, 15 (2019); https://doi.org/10.3390/biomimetics4010015
12. S.U. Rahman, S. Bilal and A.H.A. Shah, *Polymers*, **12**, 2870 (2020); https://doi.org/10.3390/polym12122870
13. M. Vellakkat and D. Hundekkal, *Mater. Res. Express*, **3**, 015502 (2016); https://doi.org/10.1088/2053-1591/3/1/015502
14. K. Pandiselvi and S. Thambidurai, *Desalination Water Treat.*, **57**, 8343 (2016); https://doi.org/10.1080/19443994.2015.1019365
15. B.S. Rathore, N.P.S. Chauhan, M.K. Rawal, S.C. Ameta and R. Ameta, *Polym. Bull.*, **77**, 4833 (2019); https://doi.org/10.1007/s00289-019-02994-7
16. A. Pawlak and M. Mucha, *Thermochim. Acta*, **396**, 153 (2003); https://doi.org/10.1016/S0040-6031(02)00523-3
17. T. Debnath, M.S. Islam, S. Hoque, P. Haque and M.M. Rahman, *J. Polymer Eng.*, **40**, 333 (2020); https://doi.org/10.1515/polyeng-2019-0312
18. M. Masoumparast, M. Mokhtary and H. Kefayati, *J. Polymer Eng.*, **40**, 342 (2020); https://doi.org/10.1515/polyeng-2019-0331
19. H. Zheng, Y.M. Du, J.H. Yu, R.H. Huang and L.N. Zhang, *J. Appl. Polym. Sci.*, **80**, 2558 (2001); https://doi.org/10.1002/app.1365
20. V. Kumar, S. Das and T. Yokozeki, *J. Polymer Eng.*, **38**, 955 (2018); https://doi.org/10.1515/polyeng-2018-0031
21. N.P.S. Chauhan, R. Ameta, R. Ameta and S.C. Ameta, *Indian J. Chem. Technol.*, **18**, 118 (2011).
22. C.-C. Huang, S.-P. Rwei, Y.-S. Huang and Y.-C. Shu, *J. Polymer Eng.*, **40**, 495 (2020); https://doi.org/10.1515/polyeng-2019-0332
23. R. Yang, Z. Wang, L. Dai and L. Chen, *Mater. Chem. Phys.*, **93**, 149 (2005); https://doi.org/10.1016/j.matchemphys.2005.03.006
24. X.J. Yang, Y. Makita, Z. Liu, K. Sakane and K. Ooi, *Chem. Mater.*, **16**, 5581 (2004); https://doi.org/10.1021/cm049025d
25. V. Sridevi, S. Malathi and C.S. Devi, *Chem. Sci. J.*, **26**, 1 (2011) .
26. A. Shyaa, O.A. Hasan and A.M. Abbas, *J. Saudi Chem. Soc.*, **19**, 101 (2015); https://doi.org/10.1016/j.jscs.2012.01.001
27. R. Karthik and S. Meenakshi, *Int. J. Biol. Macromol.*, **67**, 210 (2014); https://doi.org/10.1016/j.ijbiomac.2014.03.035
28. G. Li, C. Zhang, H. Peng, K. Chen and Z. Zhang, *Macromol. Rapid Commun.*, **29**, 1954 (2008); https://doi.org/10.1002/marc.200800501
29. F. Akbarzadeh, M. Motaghi, N.P.S. Chauhan and G. Sargazi, *Heliyon*, **6**, e03231 (2020); https://doi.org/10.1016/j.heliyon.2020.e03231
30. N.P.S. Chauhan, M. Mozafari, R. Ameta, P.B. Punjabi and S.C. Ameta, *J. Phys. Chem. B*, **119**, 3223 (2015); https://doi.org/10.1021/jp510320g
31. P. Kannusamy and T. Sivalingam, *Colloids Surf. B Biointerfaces*, **108**, 229 (2013); https://doi.org/10.1016/j.colsurfb.2013.03.015